# Numerical investigation into strong axis bending-shear interaction in rolled I-shaped steel sections

# NUMERICAL INVESTIGATION INTO STRONG AXIS BENDING-SHEAR INTERACTION IN ROLLED I-SHAPED STEEL SECTIONS

R.W.A. Dekker[a], H.H. Snijder[a] and J. Maljaars[a,b]

[a] *Eindhoven University of Technology, The Netherlands*
[b] *TNO, Delft, The Netherlands*

**Abstract**: Clause 6.2.8 of EN 1993-1-1 covers the design rules on bending-shear resistance, taking presence of shear into account by a reduced yield stress for the shear area. Numerical research on bending-shear interaction by means of the Abaqus Finite Element modelling software is presented. The numerical model is validated against the experimental results. A material model based on various tensile test coupons was used incorporating the actual material properties within the tested cross-section. Strong axis three-point bending tests were simulated by means of continuum solid elements. Good agreement was achieved between numerical and experimental result, both are compared with the EN 1993-1-1 design rule.

## 1. Introduction

Clause 6.2 of EN 1993-1-1 [1] – known as Eurocode 3 – covers the cross-sectional resistance of steel sections. The bending-shear interaction design rules assign the shear stresses to the shear area, which consists of the web and a part of the flanges. The presence of shear is taken into account by a reduced yield stress for the shear area.

This paper presents the numerical model used to investigate the bending-shear interaction in three-point-bending. This model is validated by tests. The experimental test series executed at Eindhoven University of Technology consisted of rolled HEA280, HEB240, HEM180 and IPE360 beams in steel grades S235J0+M, S355J2+M and S460J0+M bent about their strong axis and HEA280 beams bent about their weak axis. In the test series different beam lengths were used in order to invoke different shear utilization ratios. The simulation of an IPE360 beam in steel grade S355 and HEA280 beam in steel grade S460 bent about their strong axis is presented.

Bending-shear interaction is taken into account by reducing the plastic moment resistance, based on the reduction of the yield stress for the shear area. The presentation of the numerical

model is preceded by code requirements and by the results from the experimental test programme.

## 2. Design rules according to various standards

The design rules on moment-shear interaction result in a check in which the design bending moment $M$ is compared with the design value of the reduced resistance to bending allowing for the presence of a shear force ($M_V$). For the sake of comparison with the different design rules all partial factors are ignored.

The governing design rules on moment-shear interaction are listed in clause 6.2.8 of EN 1993-1-1 [1]. In case the acting shear force $V$ is less than 50% of the plastic shear resistance $V_{pl}$, the influence of shear on the bending moment resistance can be ignored. The general method is to reduce the yield stress of the shear area of the section ($A_v$) by multiplication with the reduction factor (1-ρ), as in Eq. (1).

$$f_{y,r} = (1-\rho) f_y \tag{1}$$

$f_{y,r}$ Reduced yield stress of the shear area
$\rho$ Reduction factor to determine the reduced design values of the resistance to bending moments allowing for the presence of shear forces, see Eq. (2)
$f_y$ Yield stress

$$\rho = \left(\frac{2V}{V_{pl}} - 1\right)^2 \tag{2}$$

$V$ Shear force due to loading
$V_{pl}$ Plastic shear resistance

$$V_{pl} = \frac{A_v f_y}{\sqrt{3}} \tag{3}$$

$A_v$ Shear area, see Fig. 1b for the case of rolled I-shaped sections.

In the case of rolled I-shaped sections Eurocode 3 prescribes an alternative design rule - describing the reduced plastic bending moment allowing for shear force $M_v$ - that can be used, according to Eq. (4), for the case $V > ½V_{pl}$.

$$M_V = \left[W_{pl} - \frac{\rho A_w^2}{4t_w}\right] f_y \tag{4}$$

$M_V$ Reduced bending moment allowing for shear force
$W_{pl}$ Plastic section modulus
$A_w$ Web area, see Fig. 1a
$t_w$ Web thickness

In addition to differences in the design rules, variations in the definition of the shear area are present in different standards as displayed in Fig. 1. This results in a relatively small plastic shear resistance according to DIN 188000 [2] and large shear resistance according to NEN 6770 [3], see Fig. 2.

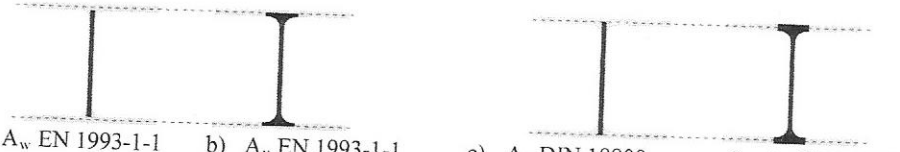

a) $A_w$ EN 1993-1-1 b) $A_v$ EN 1993-1-1 c) $A_v$ DIN 18800 d) $A_v$ NEN 6770

**Fig. 1:** Definition of web and shear area in rolled I-shaped sections

The different dimensions of an IPE360 and HEA280 beam result in differences in the moment resistances, graphically presented in Fig. 2. The differences in influence of the shear force on the plastic moment resistance between these two beams are substantial. Fig. 2 a) focuses on the influence of the size of the shear area compared to the total section area, where Fig. 2 b) focuses on the differences in Eurocode 3, DIN 188000 and NEN 6770 design rules.

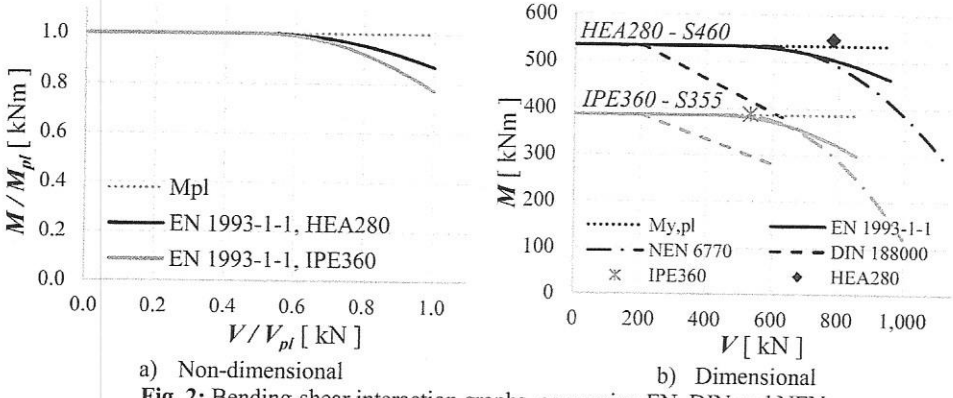


a) Non-dimensional b) Dimensional

**Fig. 2:** Bending-shear interaction graphs, comparing EN, DIN and NEN

### 2.1 Yield criterion

The reduced yield strength following clause 6.2.8 of EN 1993-1-1 [1] is in contradiction with the Von Mises yield criterion for a two dimensional stress state prescribed in clause 6.2.1. The Von Mises criterion results in Eq. (5) for combined normal and shear stress after rewriting as reduced yield stress.

$$f_{y,r} = \sqrt{1 - \left(\frac{V}{V_{pl}}\right)^2}\, f_y \tag{5}$$

Comparison between Eq. (1), (2) and (5) shows that the Von Mises yield criterion always takes shear forces into account, while the EN 1993-1-1 reduced yield stress disregards the presence of shear for $V < 0.5V_{pl}$. For $V > 0.83V_{pl}$ the reduced yield stress following Von Mises is larger than that according to Eq. (1) and Eq (2). For $V < 0.83V_{pl}$ it is the other way around.

## 3. Experimental test results

### 3.1 Test program

Tests were carried out in order to determine the cross-sectional resistance under a combination of bending and shear. The test program consisted of a total of 40 three point bending tests in both the strong and weak direction in the test set-up of Fig. 3 a). In total 27 different combinations of sections and shear utilization ratios $n = V/V_{pl}$ were tested, see Table 1. The test results were used for validation of a numerical model. This paper focuses on the test results and numerical model of two beams with a utilization ratio $n > 0.5$, ensuring a substantial influence of shear force present in the section. The HEA280 and IPE360 section selected for this purpose are indicated in bold in Table 1 and had a shear force utilization ratio of respectively $n = 0.83$ and $n = 0.67$.

The specimens were loaded by a 2 MN hydraulic pressure jack about their strong axis. The beams were provided with reusable stiffeners at the supports and a welded stiffener at mid-span. Additional plates were bolted to the mid-span stiffener to provide these in extra stiffness, see Fig 3.b). Strains were measured with 3 rosette strain gauges on the web and in total 6 linear strain gauges. The displacements were monitored on both sides of the web at mid-span and supports by means of Linear Variable Displacement Transducers (LVDTs). The measurement system is described in detail in [4].

Table 1: Test programme, 3-point strong axis bending in strong and weak axis

| Section | Steel grade | *Axis* | *# (n)* | $n=V/V_{pl}$ | $L$ (mm) |
|---|---|---|---|---|---|
| **HEA 280** | S235J0+M | strong | 7 (5) | 0.33 - 0.50 - 0.67 - 0.83 - 1.00 | 3,630 to 1,083 |
| | | weak | 6 (4) | 0.25 - 0.38 - 0.50 - 0.67 | 983 to 560 |
| | S355J2+M | strong | 7 (5) | 0.33 - 0.50 - 0.67 - 0.83 - 1.00 | 3,630 to 1,083 |
| | **S460M** | **strong** | 3 (2) | 0.67 - **0.83** | 1,790 to 1,400 |
| **IPE360** | **S355J2+M** | **strong** | 7 (4) | 0.33 - 0.50 - **0.67** - 0.83 | 2,996 to 1,095 |
| HEB240 | S355J2+M | strong | 5 (3) | 0.50 - 0.67 - 0.83 | 2,195 to 1,264 |
| HEM180 | S355J2+M | strong | 5 (4) | 0. 38 - 0.50 - 0.67 - 0.83 | 2,740 to 1,020 |

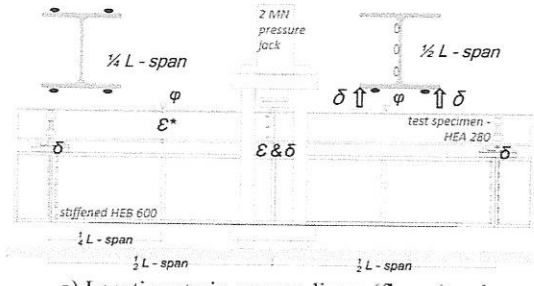


a) Location strain gauges: linear (flange) and rosette (web)

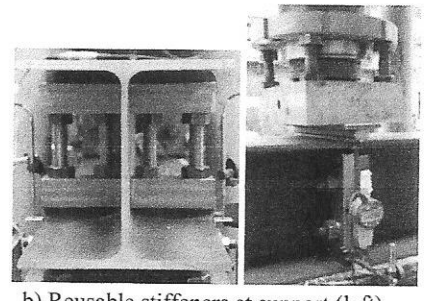

b) Reusable stiffeners at support (left), reinforced stiffener at mid-span (right)

**Fig. 3:** Strong axis bending test set-up

### 3.2 Tensile tests

Material properties were measured using tensile coupons in agreement with EN 10002-1 [5], making use of an initial strain rate of 0.00007 $s^{-1}$ which was increased in the plastic branch towards 0.00025 $s^{-1}$. The tensile tests were paused a number of times in the yield plateau and during hardening in order to obtain the velocity independent yield strength and stress-strain curve, respectively, based on the procedure described by the Technical Memorandum [6]. The Young's modulus $E$, yield strength $f_y$ and ultimate strength $f_u$ resulting from the tests are provided in Tables 2 and 3, where the final row presents the weighted average values of the entire cross-section. The true stress-plastic strain curves presented in Fig. 4 and Fig. 5 provide the influence of the position of the tensile coupons on the material properties. In both sections the web has a higher yield strength than the flanges.

### 3.3 Specimen dimension measurements

In order to be able to reproduce the test results in a numerical simulation, the specimen dimensions were measured at mid-span (B) and the beam ends (A, C) before testing, see Fig. 6.

Table 4 presents the measured height $h$, width $b$, flange thickness $t_f$, web thickness $t_w$ and root radius $r$ of the beams discussed in this paper.

Table 2: Material properties IPE360 in S355 – all dimensions in N/mm$^2$

| | $E$ | $f_y$ | $f_u$ |
|---|---|---|---|
| I_F0 | 207,225 | 366.0 | 471.4 |
| I_F1 | 212,090 | 363.8 | 581.9 |
| I_F2 | 203,230 | 376.7 | 627.2 |
| I_F3 | 211,330 | 366.2 | 480.4 |
| I_F4 | 199,690* | 357.3* | 488.3* |
| I_W0 | 205,900 | 409.6 | 623.3 |
| I_W1 | 207,200 | 425.5 | 458.1 |
| I_W2 | 205,360 | 430.2 | 615.6 |
| I_W3 | 206,970 | 427.2 | 746.4 |
| I_W4 | 207,440 | 424.0 | 694.9 |
| I_W5 | 203,190 | 403.2 | 615.2 |
| **w.av.** | **207,346** | **375.5** | **478.6** |

** Based on compression coupon and tensile test results*

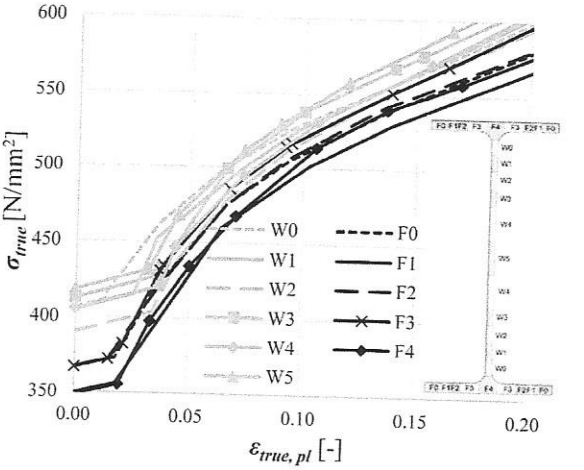


**Fig. 4:** Stress-strain curves coupons IPE360 in S355

Table 3: Material properties HEA280 in S460 – all dimensions in N/mm$^2$

| | $E$ | $f_y$ | $f_u$ |
|---|---|---|---|
| C_F0 | 217,360 | 487.9 | 595.7 |
| C_F1 | 211,470 | 483.2 | 600.0 |
| C_F2 | 218,698 | 468.6 | 605.1 |
| C_F3 | 212,355 | 466.1 | 606.5 |
| C_F4 | 205,710 | 456.6 | 604.5 |
| C_F5 | 205,090 | 433.2 | 613.6 |
| C_W0 | 206,670 | 630.4* | 678.8 |
| C_W1 | 225,385 | 490.9 | 617.8 |
| C_W2 | 208,760 | 505.7 | 620.2 |
| **w.av.** | **212,533** | **486.3** | **613.1** |

** In absence of a yield plateau the 0.2% proof stress was given*

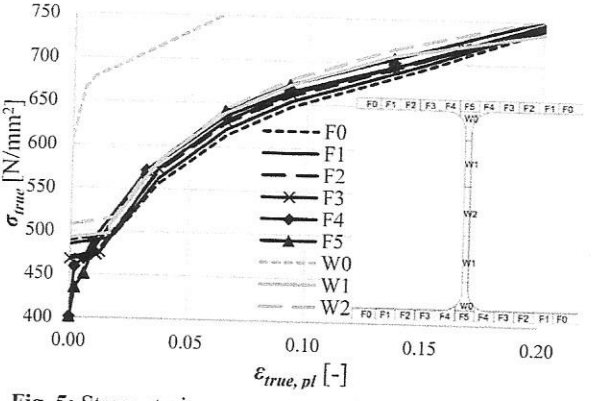


**Fig. 5:** Stress-strain curves coupons HEA280 in S460

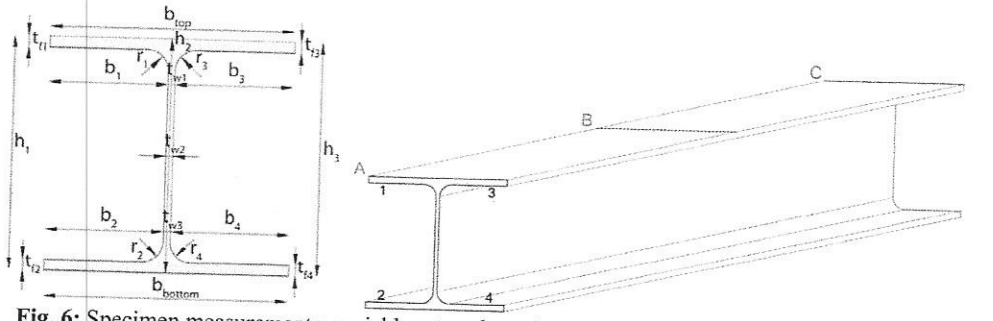


**Fig. 6:** Specimen measurements: variables at each section (left) and measurement locations (right)

Table 4: Beam measurements of specimen I3 and C2b – dimensions in mm

| Beam | $L_{beam}$ | | $h_1$ | $h_2$ | $h_3$ | $b_{top}$ | $b_{bottom}$ | $t_{f1}$ | $t_{f2}$ | $t_{f3}$ | $t_{f4}$ | $t_{w1}$ | $t_{w2}$ | $t_{w3}$ | $r$ |
|---|---|---|---|---|---|---|---|---|---|---|---|---|---|---|---|
| | | A | 360.2 | 360.2 | 361.0 | 171.2 | 170.6 | 12.1 | 12.2 | 12.2 | 12.0 | 7.2 | 7.3 | 7.5 | 18 |
| IPE360 | 2,178 | B | 360.8 | - | 361.0 | 171.1 | 170.5 | 12.1 | 12.3 | 12.2 | 12.1 | - | - | - | 18 |
| | | C | 359.8 | 360.2 | 361.2 | 171.0 | 170.6 | 12.1 | 12.3 | 12.2 | 12.1 | 7.2 | 7.4 | 7.5 | 18 |
| | | A | 275.0 | 273.6 | 273.5 | 281.0 | 281.8 | 12.5 | 12.4 | 12.3 | 12.2 | 8.2 | 8.2 | 8.1 | 23 |
| HEA280 | 1,959 | B | 275.4 | - | 273.8 | 281.1 | 281.8 | 12.4 | 12.4 | 12.3 | 12.2 | - | - | - | 23 |
| | | C | 275.7 | 273.8 | 273.5 | 281.1 | 281.9 | 12.4 | 12.4 | 12.4 | 12.2 | 8.2 | 8.1 | 8.1 | 23 |

### 3.4 Test results

Beam HEA280, S460 was loaded with an initial cross-head velocity of 1.11 mm/min which was increased to 3.33 mm/min in the plastic branch of the force-displacement curve. The experiment was executed successfully and the beam failed at a static load of 1481 kN at an in plane deflection of 5.6% of the span, see Fig. 8. In the final stages of the test large deformations of the upper flange had presented themselves. Likewise some buckling of one of the mid-span stiffeners was observed, even though additional stiffness was arranged for this stiffener.

Beam IPE360, S355 was loaded with a cross-head velocity of 0.83 up to 2.22 mm/min. This test was executed without lateral torsional buckling constraints, while in hindsight those were required. However, the test result was probably not significantly influenced by lateral torsional buckling, which is substantiated by a reference test of the same nominal dimensions but with constraints, which appeared to have an almost equal ultimate load. Beam IPE360, S355 failed at a static load of 1040 kN at an in plane deflection of 3.6% of the span, see Fig. 8.

## 4. Numerical model

The Finite Element software Abaqus [7] was used for the numerical simulations. The material properties in the numerical model were based on the true stress-strain properties resulting from the tensile coupons tests as displayed in Fig. 4 and Fig. 5 and the measured dimensions of Table 4 were used for each beam. Fig. 7 shows the boundary conditions applied, with rolling hinges over one line of nodes at the supports and a longitudinal constraint at the mid-section. At the supports the nodes of the bottom flange were tied to each other (over 10 mm length conform the stiffener thickness), creating a rigid body surface which could only rotate around the x-axis. Following the previously described method, the additional stiffness provided by plates bolted to the mid-span stiffener was modeled.

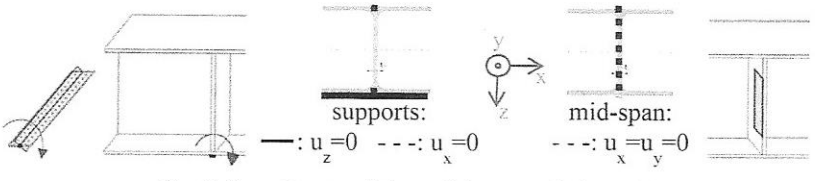


**Fig. 7:** Boundary conditions of the numerical model

Continuum (solid) elements were used in simulations, because the presence of roots is of large importance for further studies into the stress distribution in the root area. The calculation time of the quadratic elements appeared to be uneconomically large and a model with linear elements with incompatible mode formulation for preventing overstiffness due to parasitic

shear (C3D8i) appeared to provide similar resistance as quadratic elements. These elements were thus used in the study.

A mesh refinement study was executed for both sections. Because bending-shear interaction was studied, 2 and 3 elements over the thickness did not suffice and a mesh with 4 elements over flange and web thickness appeared to be required. The element width was approximately 5 times larger than the thickness and the length of the elements varied over the length of the beam. At mid-span and at the supports the length was 5 mm and away from supports and mid-span the length was 40 mm. The remainder elements varied in length, with a default configuration consisting of a gradual transition from 5 mm towards 40 mm and back to 5 mm.

The numerical simulations of the IPE360 lead to a failure load of 1065 kN - which is 102.4% of the experimental failure load - at an in plane displacement of 2.8% of the span, see Fig. 8. The corresponding bending resistance is $0.97M_{pl}$ at a shear force of $0.68V_{pl}$. In the case of the HEA280, the failure load was 1562 kN - 105.5% of the experimental failure load – at an in plane displacement of 5.5% of the span. The corresponding bending moment is $0.92M_{pl}$ at a shear force of $0.89V_{pl}$.

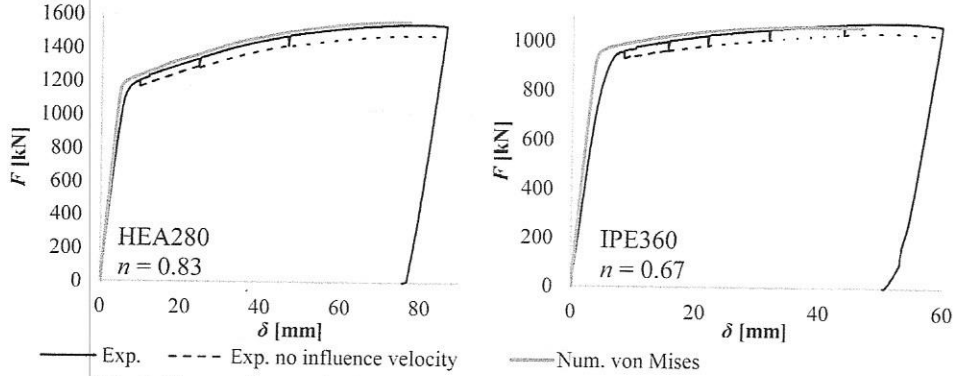


**Fig. 8:** Tests and numerical results for the HEA280 (left) and IPE360 (right) beam

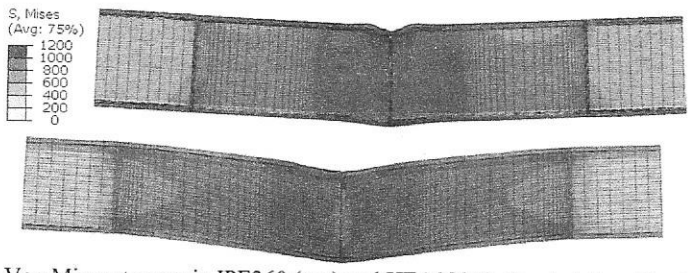


**Fig. 9:** Von Mises stresses in IPE360 (top) and HEA280 (bottom) at the ultimate load

At failure, strains of 7.8% in the longitudinal direction of IPE360 were reached on the standard position F1 (bottom flange) according to the numerical model. In HEA280 strains of 8.2% in the longitudinal direction of HEB280 were reached on the standard position F1. At the failure load shear stresses were predominantly present in the web for both sections, whereas normal stresses in longitudinal direction dominated in the root section. The progression of the Von Mises stresses corresponded with the emergence of yield lines in the experimental tests. Fig. 9 displays the Von Mises stresses at the ultimate failure load.

## 5. Conclusions

This paper presents a numerical model that is capable of simulating various configurations of I-shaped sections in 3-point bending with short spans, where shear and bending moment both influence the resistance. The main conclusions are:

1. the FEM model makes use of C3D8i elements: 4 elements over the web and flange thickness were used; the element size over the flange width and web height corresponds to 5 times the size in corresponding thickness; and in the longitudinal direction elements of 5mm depth were sufficient for the midsection see Fig. 9,
2. the numerically determined failure loads of the two sections analysed were 102.4% and 105.5% of the experimentally determined failure loads,
3. in these two FE models the shear stresses were concentrated in the web,
4. strain hardening should be considered in determination of the bending-shear resistance, since the strains at failure are significantly larger than the strains at first yield,
5. the IPE360 section reached a bending resistance of $0.97M_{pl}$ with a shear force of $0.68V_{pl}$, the HEA section a bending resistance of $0.92M_{pl}$ with a shear force of $0.89V_{pl}$ was reached, in these cases the Eurocode 3, DIN 188000 and NEN 6770 design rules are conservative, see Fig. 2.

In future research the accuracy of the EN 1993 design rule regarding bending-shear resistance will be investigated for a larger range of shear forces and sections. In addition the development of shear stresses and their location will be investigated.

## Acknowledgments

This research has received funding from the European community's Research Fund for Coal and Steel (RFCS) under grant agreements no. RFSR-CT-2013-00023. The specimens were provided by ArcelorMittal and tested at the Pieter van Musschenbroek Laboratory, Department of the Built Environment, Eindhoven University of Technology (TU/e).

## References

[1] EN 1993-1-1, *Eurocode 3: Design of steel structures- part 1-1: General rules and rules for building,* Brussels, 2011.

[2] DIN 18800-1:2009-11, *Steel structures - Part 1: Design and construction,* Berlin, Deutches Institut für Normung, 2008.

[3] NEN 6770, *TGB 1990 – Steel structures - Basic requirements and basic rules for calculation of predominantly statically loaded structures,* Delft, Nederlands Normalisatie Instituut, 1997.

[4] Dekker, RWA, Snijder HH, Maljaars J. "Experimental Study into Bending-Shear Interaction of Rolled I-shaped Sections", *Proceedings of the 13th Nordic Steel Construction Conference* (Eds.: M. Heinisuo, J. Mäkinen), Tampere, Finland, (pp. 115-116, full 10 pages paper on USB-stick), 2015.

[5] EN 10002-1 - *Metallic materials - tensile testing - part 1: Method of testing at ambient temperature,* Brussels, CEN, 2001.

[6] Zieman, RD. *Guide to Stability Design Criteria for Metal Structures*, John Wiley and Sons, 2010.

[7] *Abaqus 6.14 Online Documentation*, Dassault Systèmes, 2014.

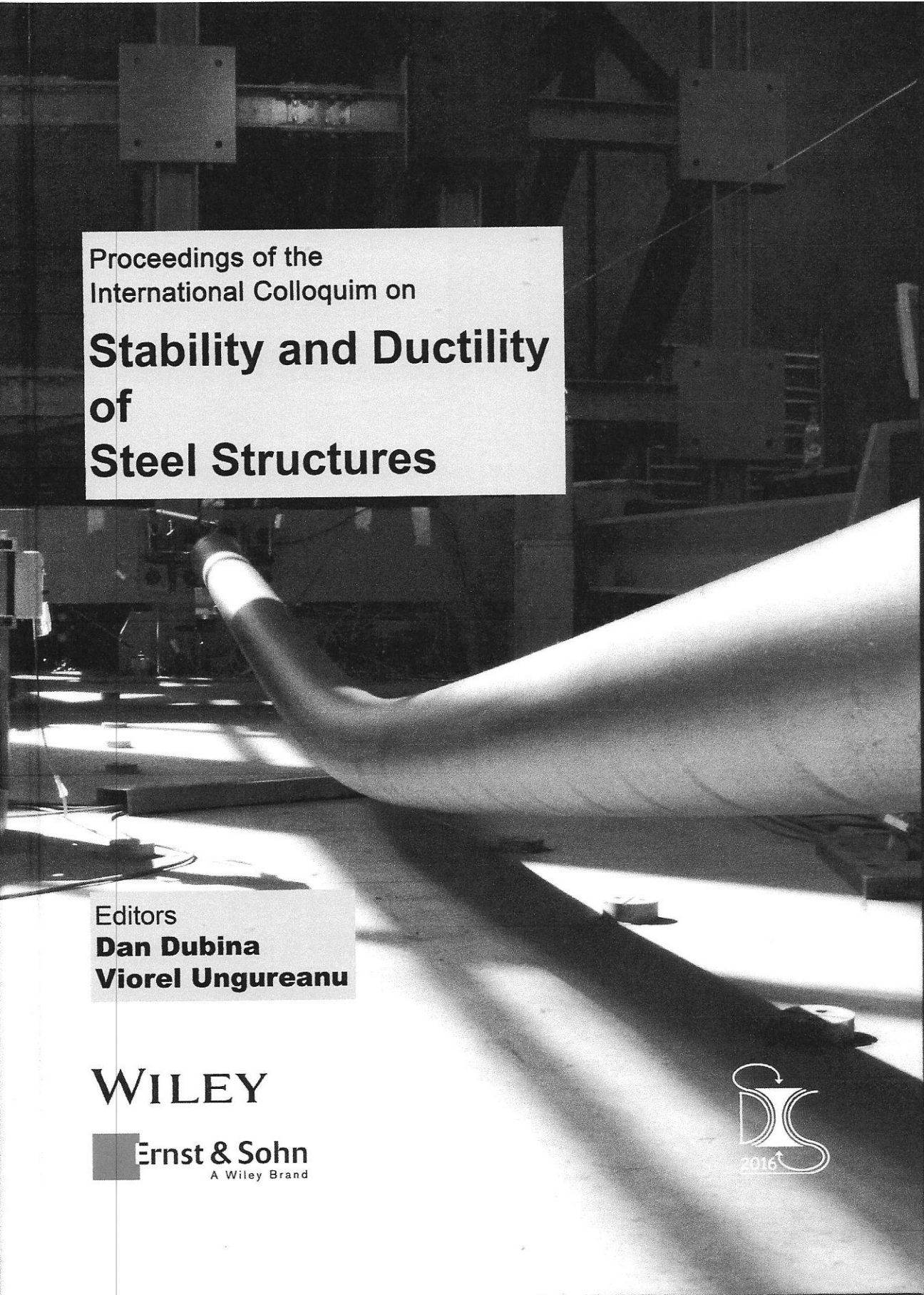

Proceedings of the
International Colloquim on

# Stability and Ductility of Steel Structures

Editors
**Dan Dubina**
**Viorel Ungureanu**

WILEY

Ernst & Sohn
A Wiley Brand

2016

**SDSS'2016**

**The International Colloquium on Stability and Ductility of Steel Structures**

30 May – 01 June 2016, Timisoara, Romania

Proceeding of the conference edited by: Dan Dubina and Viorel Ungureanu

Published by:
ECCS – European Convention for Constructional Steelwork
publications@steelconstruct.com
www.steelconstruct.com



ISBN (ECCS): 978-92-9147-133-1
Legal dep.: 408579/16 Printed in Multicomp Lda, Mem Martins, Portugal